Bioactive borosilicate glass scaffolds: improvement on the strength of glass-based scaffolds for tissue engineering

Xin Liu · Wenhai Huang · Hailuo Fu · Aihua Yao ·
Deping Wang · Haobo Pan · William W. Lu

Abstract Three-dimensional macroporous scaffolds with the pore size of 200–500 μm were fabricated by replication method using bioactive borosilicate glass from Na_2O–K_2O–MgO–CaO–SiO_2–P_2O_5–B_2O_3 system. The effects of the strength of the strut in reticulated scaffold, as well as the geometrical parameter of the scaffold on the strength of reticulated scaffold were investigated. Scanning electron microscope (SEM) and X-ray diffraction (XRD) results show that the solidified glass struts in the reticulated scaffold could be obtained through a sufficient vicious flow of glass, during the fabrication. By increasing the solid content in slurries, from which the scaffold was made, the load-bearing units of the reticulated scaffold switch from struts to the walls between the pores, and the compressive strength dramatically climbs higher than the theoretical strength calculated by Gibson model. In particular, the compressive strength of the reticulated scaffold, as high as ∼10 MPa with the porosity of ∼70%, is close to the reported compressive values of human cancellous bone. This indicates the bioactive borosilicate glass-based scaffold is a promising candidate for bone tissue engineering.

X. Liu · W. Huang (✉) · H. Fu · A. Yao · D. Wang
Institute of Bioengineering and Information Technology
Materials, Tongji University, Shanghai 200092,
People's Republic of China
e-mail: whhuang@mail.tongji.edu.cn; huangwe@mst.edu

H. Pan · W. W. Lu
Faculty of Medicine, University of Hong Kong,
Hong Kong 999077, People's Republic of China

1 Introduction

Scaffold served as a temporary macroporous three-dimensional template is believed to benefit the proliferation of osteoblasts and the formation of bone-extracellular matrix. Therefore, an ideal scaffold should at least have the following characteristics: (i) highly porous structure with interconnected pore network for cell growth and flow transportation of nutrients and metabolic waste; (ii) biocompatibility and bioresorbabilty with controllable degradation and resorption rate to match cell/tissue growth in vitro and/or in vivo; (iii) suitable surface chemistry for cell attachment and proliferation (iv) mechanical properties to match those of the tissues at the site of implantation [1]. To meet the requirements of ideal scaffolds, the bioactive glasses as well as other bioactive materials, e.g., calcium phosphates, have already been studied for many years [2–4], including the dissolution behavior in vitro [5]. Although many techniques have been employed in the fabrication of porous scaffolds such as foaming, phase separation and sol–gel method, the replication method is showing extraordinary attention, due to easily fabrication of larger pore size up to several hundred micrometers [6–8].

However, these porous structures always suffer the dilemma of lower mechanical strength, thus unfortunately inhibiting its further application. Although many attempts have already been tried to improve it, it is still a big challenge to obtain a high mechanical strength together with a high porosity. Based on above problem, an open-cell cubic body model developed by Gibson [9] has been employed in replication method [10, 11]. According to Gibson model, the strength of struts in the scaffold and geometrical morphologies of scaffold are dominant factors to determine the strength of reticulated scaffold. Therefore, several attempts have been proposed, such as decreasing

the defects in the struts by degassing [12], introducing a second-phase for reinforcement [13–15] or increasing the strut thickness by repeating soak process [16]. However, even so the measured mechanical strength of ceramic-based scaffold by replication method is still unsatisfied, only around 0.2–1.1 MPa [17, 18], significantly lower than cancellous bone, around 4–12 MPa [19, 20]. Besides, although this technique has been widely applied to produce ceramic-based porous scaffold, seldom attempt has been made in bioactive glass-based scaffold [6]. Even worse, the compressive strength of a 45S5 Bioglass® based scaffold was reported only around 0.3–0.4 Mpa, due to crystallization during the preparation process [6].

Therefore, in order to avoid the undesired crystallization, an appropriate sintering temperature has to be selected. As reported by Brink [21], the sintering temperature could be decreased by adding potassium oxide, magnesium oxide or boron oxide, in order to widen the working temperature range. The previous studies have already shown better bioactivity and controllable degradation of borosilicate glass (Na_2O–K_2O–MgO–CaO–SiO_2–P_2O_5–B_2O_3) in vitro test if sodium oxide was partially substituted by potassium oxide, calcium oxide was partially replaced by magnesium oxide, and silicon oxide was partially or totally replaced by boron oxide [5, 22]. Based upon above attempts, the objective of this work is therefore to fabricate borosilicate scaffold with good thermal workability from Na_2O–K_2O–MgO–CaO–SiO_2–P_2O_5–B_2O_3 glass system and to explore the key parameters that determine the strength of scaffold. In particular, the influence of thermal behavior of glass, the strut strength as well as the geometrical parameter of the structure on the compressive strength will be highlighted.

2 Experiment procedures

2.1 Synthesis

Borosilicate glass with the composition of $6Na_2O$–$8K_2O$–$8MgO$–$22CaO$–$36B_2O_3$–$18SiO_2$–$2P_2O_5$ mol%, designated as D-Alk-B glass (Double alkali borate glass), was prepared by melting the mixture of Na_2CO_3, K_2CO_3, $MgCO_3$, $CaCO_3$, H_3BO_3, SiO_2, and $NaH_2PO_4 \cdot 2H_2O$ (analytical grade, Sinopharm Chemical Reagent Co., Ltd. China) in a platinum crucible at 1150°C in the silicon carbide rod furnace (SSX-12–16; Shanghai Laboratory Electric Furnace Works. China). After 2 h, the melting mixture was quenched between cold stainless-steel plates, and then crushed and sieved, to select the glass powders with the average diameter of ~4 μm. These powders were added and stirred in pure ethanol solution (analytical grade, Sinopharm Chemical Reagent Co., Ltd., China) as the source to fabricate scaffold.

Then, the ethyl-cellulose (EC, analytical grade, Sinopharm Chemical Reagent Co., Ltd., China) was added to ensure a well dispersion of the glass particles, as listed in Fig. 1. The solution was stirred vigorously for 5 h, to prepare the slurries for the impregnation. The solid content of the slurry was adjusted by the amount of ethanol, according to the ratio of EC/glass powder (Fig. 1).

The polyurethane foams (Shanghai No. 6 Plastic Co., Ltd; China) with open porosity of approximately 50 pores per inch were cut into Φ14 mm × 10 mm for impregnation as the polymer templates. Then, the foams were immersed in the prepared slurry. Excess slurry was squeezed out, leaving a more homogeneous coating on the foam struts. The foams coated by slurry were dried at room temperature for ~24 h, until no change of weight was measured. The green body was gradually heated from room temperature to 400°C at the speed of 1.5°C min⁻¹, holding 2 h to allow the complete pyrolysis of polyurethane foam, and then further increased to 550°C at a speed of 2.5°C min⁻¹, holding another 2 h. Finally, cooling down to room temperature, the porous D-Alk-B scaffold was then obtained.

In addition, another composition of the glass ($24.4Na_2O$–$26.9CaO$–$30.73B_2O_3$–$15.37SiO_2$–$2.6P_2O_5$ mol%, designated as 45S5-B) based on 45S5 Bioglass® was selected as control group by replacing 66.7% of SiO_2 with B_2O_3. No change of preparation process was made, except higher sintering temperature was chosen at 750°C for 2 h in order to increase the liquid phase amount during sintering.

2.2 Characterizations

The ratio of the apparent density of green body to the solid glass density, called relative density ratio of green body R_{gb}, was used to quantitatively monitor the slurry coating on the foams. The weight (g) of slurry coating on the foam was measured by the change of weight between dried green body ω_{gb} and original foam ω_{foam}. The volume of the green
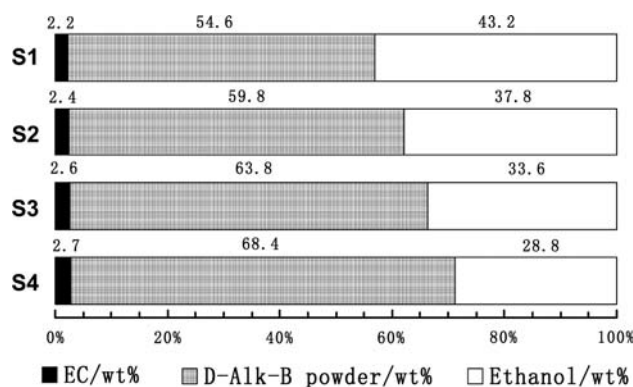

Fig. 1 Compositions of slurries studied in the experiment

body can be calculated by ω_{foam}. Thus, R_{gb} could be calculated by:

$$R_{gb} = \left[(\omega_{gb} - \omega_{foam}) \cdot \left(\frac{\omega_{foam}}{\omega_{foam}} \right)^{-1} \right] \cdot \rho_{solid}^{-1}$$
$$= \frac{(\omega_{gb} - \omega_{foam})\rho_{foam}}{\omega_{foam} \cdot \rho_{solid}} \tag{1}$$

where the density of annealed solid D-Alk-B glass is $\rho_{solid} = 2.6 \text{ g cm}^{-3}$.

The apparent density of scaffold $\rho_{scaffold}$ was determined by Archimedes method, using kerosene as the solution medium due to the high chemical activity of D-Alk-B scaffold in water. The open porosity p and the relative density ratio of scaffold $R_{scaffold}$ was then calculated by:

$$p = 1 - R_{scaffold} = 1 - \frac{\rho_{scaffold}}{\rho_{solid}} \tag{2}$$

Then the shrink rate θ_s determined by the discrepancy between V_{gb} and $V_{scaffold}$ could be calculated by:

$$\theta_s = \frac{V_{gb} - V_{scaffold}}{V_{gb}} = (R_{gb}^{-1} - R_{scaffold}^{-1}) \cdot R_{gb}^{-1} = 1 - \frac{R_{gb}}{R_{saffold}} \tag{3}$$

where V_{gb} and $V_{scaffold}$ were the volume of the green body and the scaffold, respectively.

The compressive strength of the scaffold was tested on a tensile testing machine (CMT6104; SANS Testing Machine Inc. China) at a crosshead speed of 0.5 mm min^{-1}. The modulus of rupture of solid glass was determined from a three-point bending test, using the annealed bulk glass specimens with the dimension of 5 mm × 5mm × 60 mm. The modulus of rupture σ_r is evaluated as:

$$\sigma_r = \frac{3FL}{2wh^2} \tag{4}$$

where F was the critical fracture load, w and h were, respectively expressed as the width and the thickness of the specimen. L was the span length, where $L = 40$ mm.

The glass transition temperature T_g and the devitrification temperature T_d of the D-Alk-B and 45S5-B glasses were investigated by differential thermal analysis (DTA; STA 449 C; NETZSCH Corp. German) performed on finely powdered glass samples. Bulk D-Alk-B and 45S5-B solid glass specimens of one inch in length were prepared to determine the thermal expansion behavior and the softening temperature by a dilatormeter (Model 1600; Orton, Columbus, OH. USA).

The microstructure of scaffold was characterized by scanning electron microscopy (SEM; Quanta 200 FEG; FEI Co. Japan). The phase composition of as-received glass and scaffold was determined by X-ray diffraction (XRD; D/max 2550; Rigaku International Corp. USA).

3 Result and discussion

3.1 Theoretical model

To better understand the mechanical behavior of porous scaffold, a theoretical model proposed by Gibson [9] is quite often used. A cubic cell is regarded as the basic unit in this model. The failure of the open-cell bodies under uniaxial stress is considered to be primarily caused by bending of the cell edges. Thus, the theoretical compressive strength σ_{tc} can be estimated by the cell geometrical parameter t/l of the scaffold, which is expressed as followed [9]:

$$\frac{\sigma_{tc}}{\sigma_{fs}} \propto (t/l)^3 \tag{5}$$

where σ_{fs} is the modulus of rupture of the solid material, t is strut thickness and l is strut length.

The relative density ratio of scaffolds is proportional to the square of the ratio of the strut thickness to length, given by [9]:

$$R_{scaffold} = \frac{\rho_{scaffold}}{\rho_{solid}} = C_1 (t/l)^2 \tag{6}$$

where C_1 is a constant.

Combining the Eqs. 2, 5, and 6, the theoretical compressive strength can be then determined by the porosity of scaffolds p as followed:

$$\frac{\sigma_{tc}}{\sigma_f} = C_2 (1 - p^{3/2}) \tag{7}$$

where $C_2 = 0.2$ for brittle crushing suggested by Gibson.

Therefore, according to Eq. 7, the theoretical strength of scaffold with different porosities can be calculated by σ_{fs}. In the present work, the modulus of rupture σ_{fs} of the annealed D-Alk-B and 45S5-B glass was tested as 86.2 ± 12.5 MPa and 43 ± 5.2 MPa, respectively. The theoretical compressive strength σ_{tc} (in MPa) calculated by Gibson model is then calculated by:

$$\sigma_{tc} = 17.2(1 - p)^{3/2} \tag{8}$$

for D-Alk-B scaffolds, and

$$\sigma_{tc} = 8.6(1 - p)^{3/2} \tag{9}$$

for 45S5-B scaffolds, respectively.

3.2 Strut strength

As shown from Eq. 5, the modulus of rupture σ_{fs}, representing the strut strength, is crucial to determine the final strength of the scaffold. To eliminate defects and cracks preexisted in the struts of green bodies, sintering is a crucial step. For glass-based material, the sintering of glass particles was accomplished by the vicious flow of glass.

The presence of a liquid reduces the pores between particles, and bonds the solid glass particles together [23]. Consequently, a favorable glass viscosity should be guaranteed for the sintering of glass-based scaffolds.

As shown in Fig. 2a, the linear thermal expansion curve of D-Alk-B bulk glass displays a significant change of slope occurring at 519°C, corresponding to the glass transformation temperature T_g. The dilatometric softening temperature T_d of the glass was at 570°C and the onset temperature of the first crystallization peak T_{onset} is occurred at 660°C. Therefore, the sintering temperature of 550°C was then selected for D-Alk-B scaffold, because an appropriate temperature should be between T_g and T_{onset}, in order to avoid crystallization.

As shown in Fig. 2b, the glass transition temperature T_g and softening temperature T_d of 45S5-B are 463 and 493°C, respectively. The slope changed slightly at the transition temperature point, comparing with D-Alk-B glass, indicating less glass fluid and higher glass viscosity during the glass transition. Therefore, the sintering temperature of 45S5-B glass higher than softening temperature T_d was necessary, due to insufficient glass vicious flow between T_g and T_d. However, the softening temperature (493°C) was much closer to the onset temperature (504°C) of crystallization, thus only an extremely narrow range of sintering temperature could be applied. Even worse, the vicious flow in such temperature was still limited. Therefore, a higher temperature of 750°C was finally selected for 45S5-B scaffold in order to enhance the amount of glass fluid.

The microstructures of the sintered scaffold are shown in Fig. 3. Although D-Alk-B and 45S5-B scaffold were both prepared from the slurry composition of S2, the surface roughness are significantly different. As shown in Fig. 3a, the surface of the D-Alk-B scaffold is very smooth. The cross-section of the strut was dense, in despite of a few number of closed pores trapped in it. This phenomenon indicated that large number of defects and cracks, which preexisted in the coated green bodies, had already been effectively removed by the adequate vicious flow of glass during sintering. On the other hand, the surface of the 45S5-B scaffold seemed to be rough, as shown in Fig. 3b.
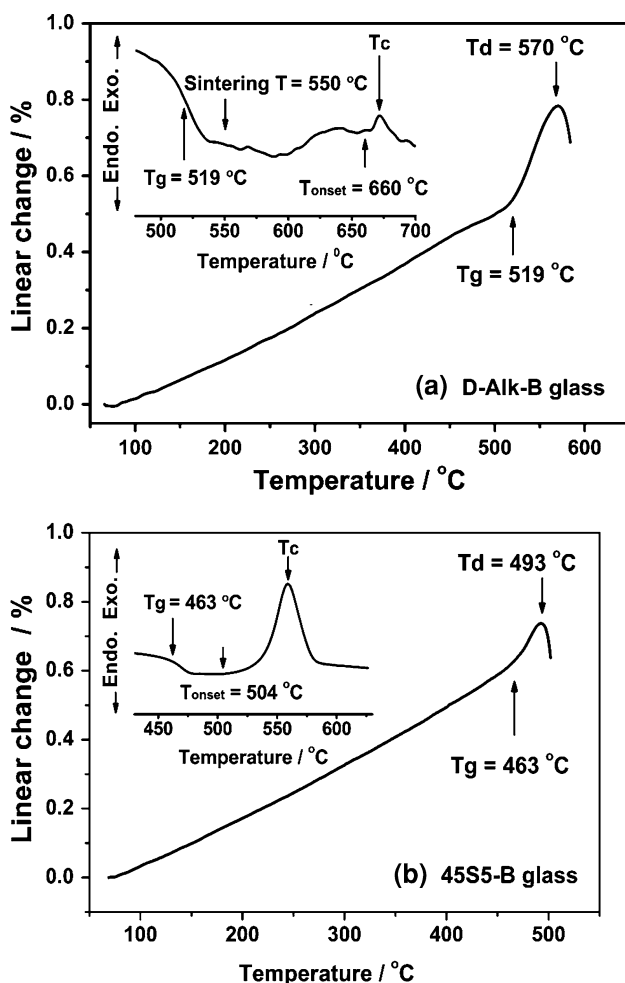

Fig. 2 Thermal expansion curves of (a) D-Alk-B glass and (b) 45S5-B glass. Inlet in the graph is the DTA curve
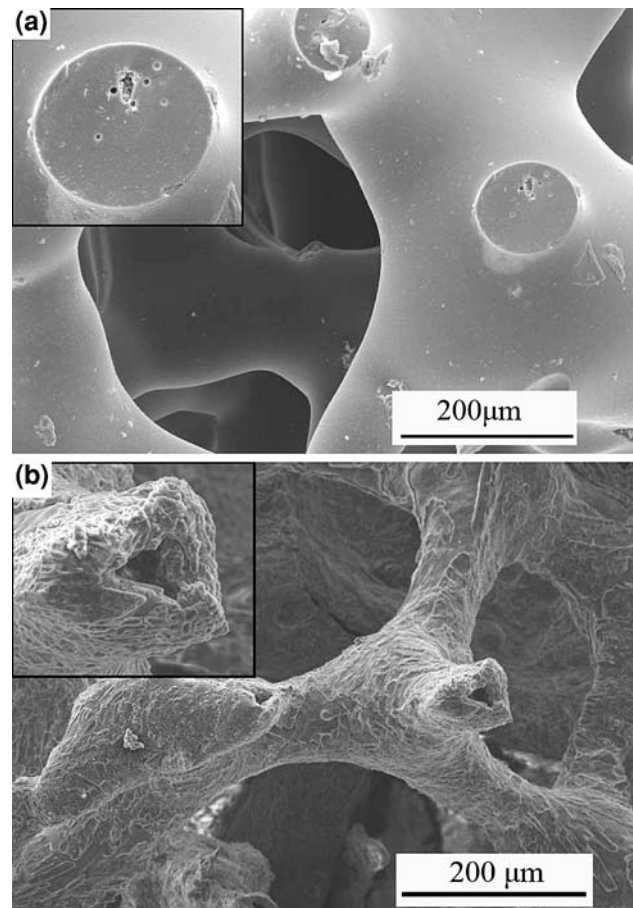

Fig. 3 SEM micrographs of (a) D-Alk-B scaffolds and (b) 45S5-B scaffolds after sintering

A closer look at the cross-section of a single strut indicated that the particles were loosely bonded and a large number of cracks and defects still existed in the struts, where the hollow structure significantly decreased its mechanical strength.

XRD patterns shown in Fig. 4a display no significant crystallization in D-Alk-B scaffold even after sintering at 550°C, while a well-crystallinzed structure is detected as $CaNa_3B_5O_{10}$ in 45S5-B scaffold after sintering at 750°C. As we known, the crystallization of glass will dramatically affect the strut strength of the scaffold. Thus, the controlled crystallization might be helpful, however, the uncontrolled crystallization would not only deteriorate the mechanical properties [24], but also might severely inhibit the glass vicious flow. As indicated in Fig. 3b, the higher viscosity caused by the crystallization of 45S5-B glass severely inhibited the removal of pores between the glass particles. Therefore, the hollow structure was detected as a typical morphology for porous ceramic materials, while the ceramic particles were sintered [11, 12].

The theoretical strength of scaffold was calculated by Eqs. 8 and 9, to assess the experimental values. As shown in Fig. 5, the measured strength for D-Alk-B scaffold is approximately close to the theoretical strength predicted by Gibson model, while the measured strength of 45S5-B scaffold is significantly less than the theoretical strength calculated by Gibson model. Besides, it has to be strengthened that the theoretical strength of D-Alk-B scaffold is really much higher than 45S5-B, due to the intrinsic higher strength of D-Alk-B glass itself.

3.3 Geometrical parameter of scaffolds

According to Eq. 5, not only strut strength, but the geometrical parameter t/l may affect the strength of scaffold. In the present work, the strut thickness t was adjusted by the solid content in the slurry. As shown in Table 1, the relative density ratio of green body increases from slurry S1 to S4 by enhancing solid content, indicating that the strut coated with thicker slurry. The strut length of green bodies was nearly the same as employed templates. However, the strut length l of the sintered scaffold might decrease slightly, due to the greater shrinkage rate of heavier-coated green bodies. As a result, the geometrical parameter increased with the increase of solid content, finally leading to the improvement of its compressive strength.

Meanwhile, it is noticeable that the scaffold of S4 yielded a compressive strength of about 10 MPa, close to the reported values of human cancellous bone, which is 4–12 MPa [19, 20]. The comparison between the experimental strength and the theoretical value shown in Fig. 6 indicated that the compressive strength dramatically soared
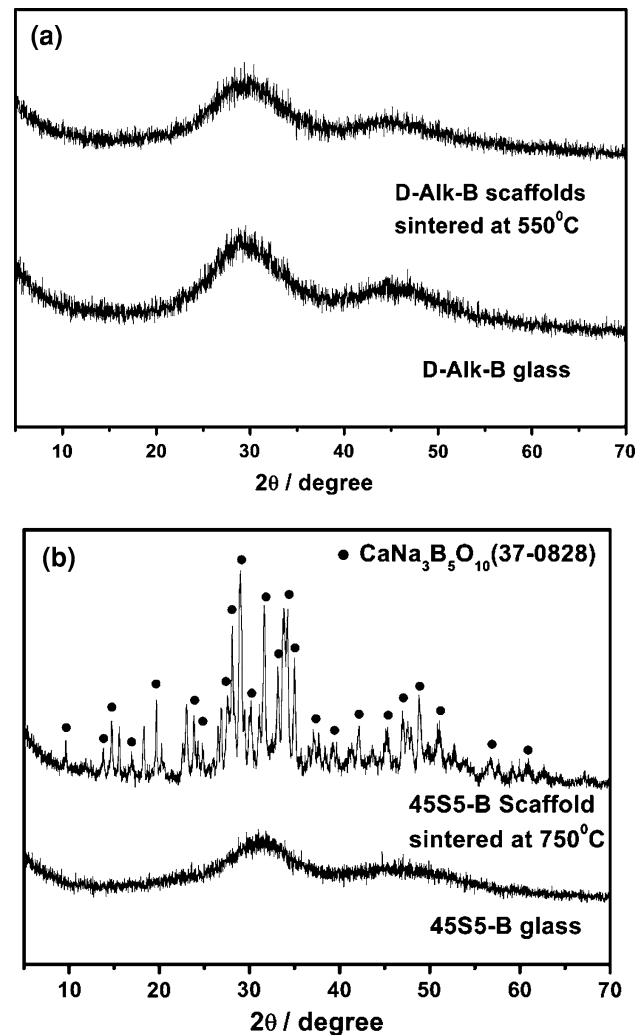

Fig. 4 XRD spectra of (**a**) D-Alk-B glass and (**b**) 45S5-B glass before and after sintering
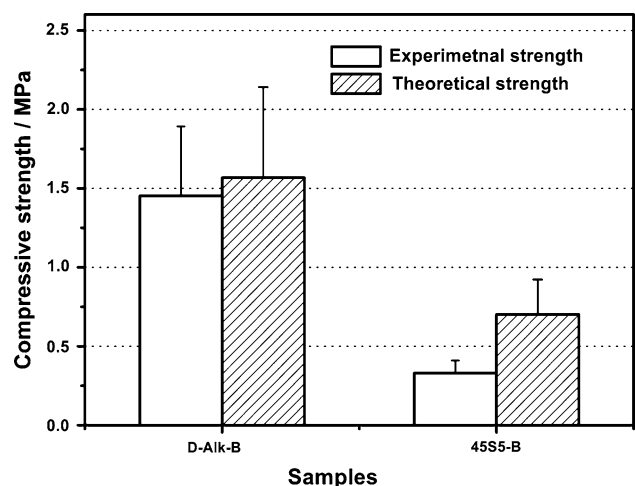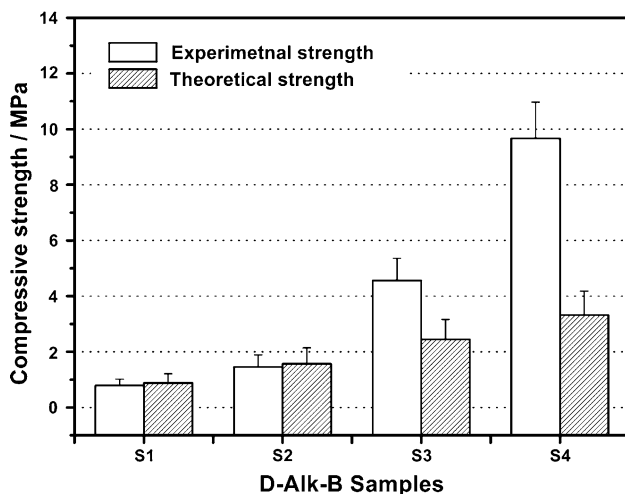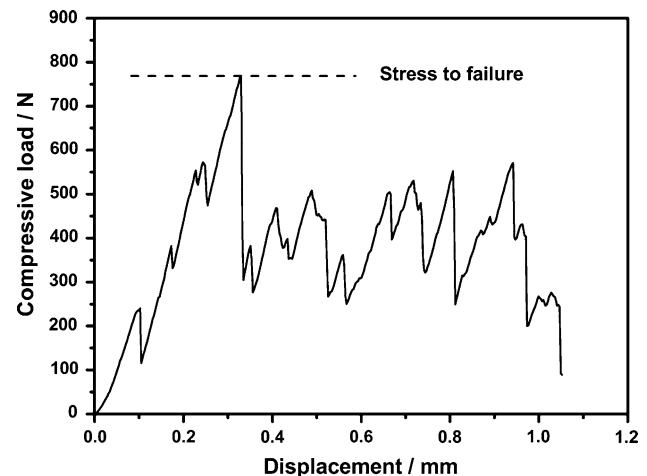

Fig. 5 Comparisons between the theoretical compressive strength and experimental strength of D-Alk-B and 45S5-B scaffolds prepared from slurry with solid content of 62.2 wt%

Table 1 Parameters of scaffolds

Sample	Solid content (wt.%)	Relative density ratio of green body (%)	Compressive strength of scaffolds (MPa)	Porosity of scaffolds (%)	Shrinkage rate θ_s (%)	Relative geometrical parameter of scaffolds ε_g
S1	56.8	6.6	0.8 ± 0.2	86.7 ± 2.2	50.2 ± 7.2	1
S2	62.2	8.1	1.5 ± 0.4	80.4 ± 3.1	58.6 ± 8.2	1.21 ± 0.01
S3	66.4	9.9	4.6 ± 0.8	73.3 ± 2.8	62.9 ± 4.6	1.41 ± 0.05
S4	71.1	12.1	9.7 ± 1.3	67.7 ± 2.6	63.3 ± 3.2	1.57 ± 0.07

up, even much higher than the theoretical calculation with the increasing relative density ratio of green bodies. The typical compressive load versus displacement curve of compressive strength test for D-Alk-B scaffolds, as shown in Fig. 7, displays some stress-concentrated sites cracked first, with the load slowly applied on the scaffold, causing minor stress drop on the curve. However, the failure of these few sites did not prevent the stress from increasing on the whole construct, and the other sites could survive a maximum stress. The maximum stress caused a sever fracture of the scaffold and a sharp stress drop. The followed compressive load-displacement relationship also gave out the similar jagged curve, but the stresses at peak points were lower than the maximum stress. The compressive strength was, therefore, determined by the maximum stress. In the case of the scaffold from S4 sample, the maximum compressive load could reach as higher as about 768 N as shown in Fig. 7, which is mainly attributed to the change of microstructures of these scaffolds.

The three-dimensional interconnected porous structures of scaffolds by different solid content were shown in Fig. 8, with the pore size around 200–500 μm. Although diminished slightly, owing to the increased shrinkage rate, the pore diameter remained around 200–300 μm of S4

Fig. 7 Typical compressive load-displacement curve of the D-Alk-B scaffold prepared from S4

scaffold, larger than the minimum size of approximately 100 μm, which were considered to be the limit for osteo-conduction in bone graft applications [25]. In particular, it is necessary to point out that the struts of scaffold grew thicker as the increase of solid content. The walls of pores were gradually formed and occupied by glass. The basic units of the scaffold gradually changed from struts to the walls of pores.

According to Eqs. 2 and 6, the geometrical parameter t/l can be estimated by the porosity. Taking the value of S1 geometrical parameter as one unit, the relative geometrical parameter ε_g of S2, S3, and S4 can be determined, as listed in Table 1. Since these scaffolds are all based on D-Alk-B glass, given σ_{fs} a constant, the Eq. 5 can be then expressed as:

$$\log(\sigma_{tc}) = 3 \log \varepsilon_g + C_3 \qquad (10)$$

where C_3 is a constant. Therefore, the theoretical slope of the $\log(\sigma_{tc}) - \log \varepsilon_g$ curve should be three.

It was found that the slope of experimental curve was nearly parallel to curve of Gibson model in area I, as shown in Fig. 9, indicating that the increase of compressive strength is mainly attributed to the increase of strut thickness and the decrease of pore size. Although significantly deviated from the theoretical calculation, the slope in area

Fig. 6 Theoretical and experimental compressive strength of scaffolds

Fig. 8 SEM micrographs of scaffolds prepared from slurries with different composition of S1 (**a**), S2 (**b**), S3(**c**), and S4 (**d**)
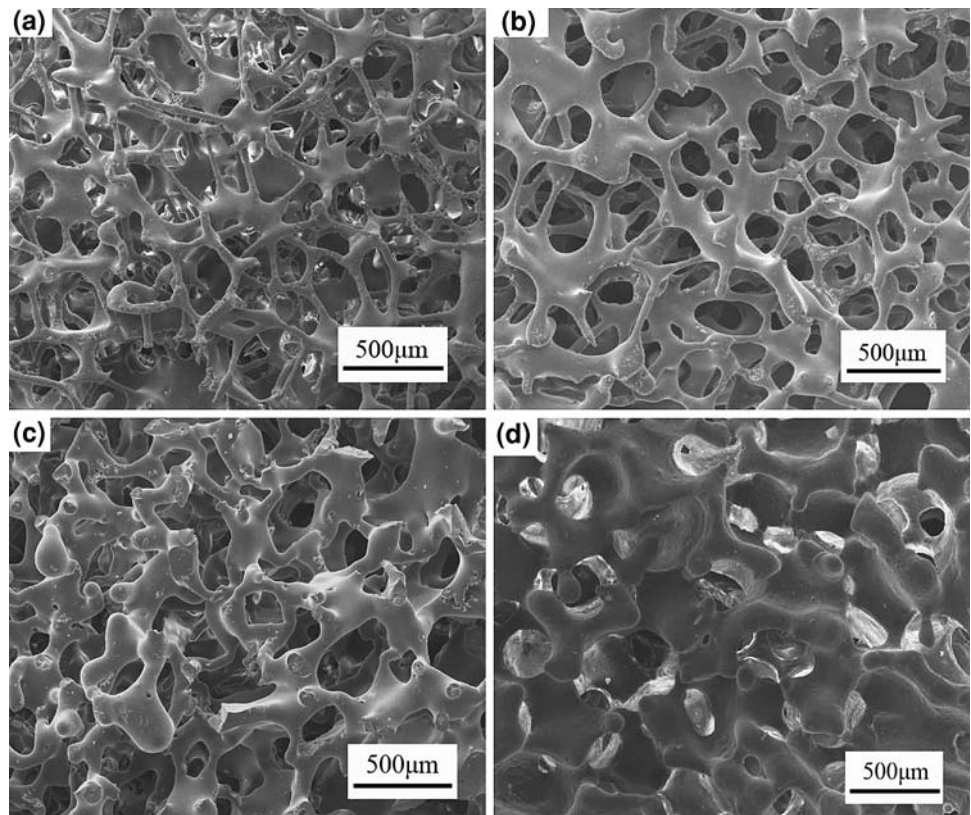
II still increased steadily, because the load-bearing unit of scaffold switched from the struts to the walls of pores, thus requiring greater force to break it. Therefore, comparing with Gibson model, the structure change from struts to walls seems to be more effective to enhance the strength of scaffold.
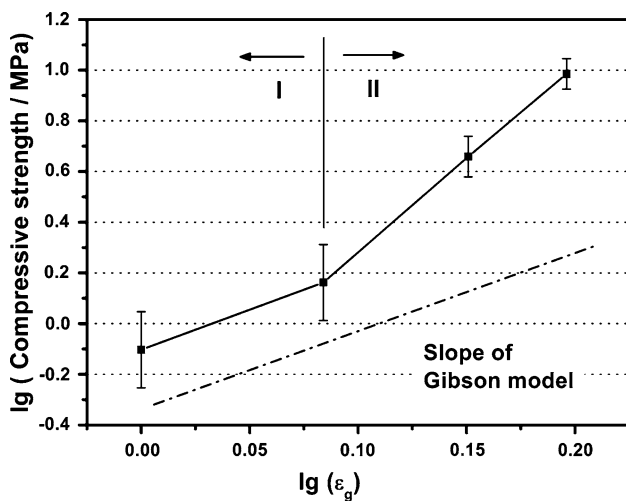

Fig. 9 Dependence of compressive strength with relative geometrical parameter, dash line is from Gibson model; I-area—Strut-structure dominated; II-area—Wall structure dominated

4 Conclusions

Reticulated borosilicate scaffold with three-dimensional interconnected structure was successfully prepared by replication technique. XRD and SEM results show that D-Alk-B glass is suitable to produce adequate vicious flow during sintering and to obtain dense and smooth struts with good thermal workability. The compressive strength of D-Alk-B scaffold prepared in this study is close to the theoretical value predicted by Gibson model. In particular, higher strength up to ~ 10 MPa ($\sim 70\%$ porosity) could be achieved by thicker coated green bodies, thus switching the load-bearing units from the struts to the walls between pores. Therefore, bioactive borosilicate scaffold can be favored as a promising candidate for tissue engineering.

References

1. D.W. Hutmacher, Biomaterials **21**, 2529 (2000). doi:10.1016/S0142-9612(00)00121-6
2. J.R. Jones, L.M. Ehrenfried, L.L. Hench, Biomaterials **27**, 964 (2006). doi:10.1016/j.biomaterials.2005.07.017

3. W. Liang, M.N. Rahaman, D.E. Day, N.W. Marion, G.C. Riley, J.J. Mao, J. Non-Cryst. Solids **354**, 1690 (2008). doi:10.1016/j.jnoncrysol.2007.10.003

4. Y. Zhang, M.Q. Zhang, J. Biomed. Mater. Res. **61**, 1 (2002). doi:10.1002/jbm.10176

5. S. Roy, B. Basu, J. Mater. Sci.: Mater. Med. **19**, 3123 (2008). doi:10.1007/s10856-008-3440-3

6. Q.Z. Chen, I.D. Thompson, A.R. Boccaccini, Biomaterials **27**, 2414 (2006). doi:10.1016/j.biomaterials.2005.11.025

7. C. Vitale-Brovarone, E. Verne, L. RoD-Alklio, P. Appendino, F. Bassi, G. Marinasso, G. Muzio, R. Canuto, Acta Biomater. **3**, 199 (2007). doi:10.1016/j.actbio.2006.07.012

8. D. Baksh, J.E. Davies, S. Kim, J. Mater. Sci.: Mater. Med. **9**, 743 (1998). doi:10.1023/A:1008959103864

9. L.J. Gibson, J. Biomech. **38**, 377 (2005). doi:10.1016/j.jbiomech.2004.09.027

10. L. Montanaro, Y. Jorand, G. Fantozzi, A. Negro, J Eur Ceram Soc **18**, 1339 (1998). doi:10.1016/S0955-2219(98)00063-6

11. F.A. Costa Oliveira, S. Dias, M. Fátima Vaz, J. Cruz Fernandes, J. Eur. Ceram. Soc. **26**, 179 (2006). doi:10.1016/j.jeurceramsoc.2004.10.008

12. X.W. Zhu, D.L. Jiang, S.H. Tan, Mater. Lett. **51**, 363 (2001). doi:10.1016/S0167-577X(01)00322-6

13. F. Helmann, O.C. Standard, F.A. Müller, M. Hoffman, J. Mater. Sci.: Mater. Med. **18**, 1817 (2007). doi:10.1007/s10856-007-3028-3

14. Y.U. Kim, M.C. Kim, K.N. Kim, K.M. Kim, S.H. Choi, C.K. Kim et al., Key Eng. Mater. **284/286**, 313 (2005)

15. I.K. Jun, J.H. Song, W.Y. Choi, Y.H. Koh, H.E. Kim, H.W. Kim, J. Am. Ceram. Soc. **90**, 2703 (2007). doi:10.1111/j.1551-2916.2007.01762.x

16. Y.S. Park, K.N. Kim, K.M. Kim, S.H. Choi, C.K. Kim, R.Z. Legeros et al., J. Mater. Sci. **41**, 4357 (2006). doi:10.1007/s10853-006-6261-0

17. K. Rezwan, Q.Z. Chen, J.J. Blaker, A.R. Boccaccini, Biomaterials **27**, 3413 (2006). doi:10.1016/j.biomaterials.2006.01.039

18. C. Wu, J. Chang, W. Zhai, S. Ni, J. Wang, J. Biomed. Mater. Res. B Appl. Biomater. **78**, 47 (2006). doi:10.1002/jbm.b.30456

19. E.B.W. Giesen, M. Ding, M. Dalstra, T.M.G.J. van Eijden, J. Biomech. **34**, 799 (2001). doi:10.1016/S0021-9290(01)00030-6

20. Y.N. Yeni, D.P. Fyhrie, J. Biomech. **34**, 1649 (2001). doi:10.1016/S0021-9290(01)00155-5

21. M. Brink, J. Biomed. Mater. Res. **36**, 109 (1997). doi:10.1002/(SICI)1097-4636(199707)36:1<109::AID-JBM13>3.0.CO;2-D

22. A.H. Yao, D.P. Wang, W.H. Huang, F. Qiang, N.R. Mohamed, D.E. Day, J. Am. Ceram. Soc. **90**, 303 (2007). doi:10.1111/j.1551-2916.2006.01358.x

23. J.S. Reed, *Principles of Ceramics Processing* (Wiley, New York, 1995), pp. 596–609

24. D.C. Clupper, L.L. Hench, J. Non-Cryst. Solids **318**, 43 (2003). doi:10.1016/S0022-3093(02)01857-4

25. S.F. Hulbert, S.J. Morrison, J.J. Kawitter, J. Biomed. Mater. Res. **6**, 347 (1972). doi:10.1002/jbm.820060505